Graphene Photonics, Plasmonics, and Optoelectronics

Phaedon Avouris, *Senior Member, IEEE*, and Marcus Freitag

(Invited Paper)

***Abstract*—We review the characteristics of the optical excitations of graphene involving interband, intraband, and collective (plasmon) electronic excitations. We then discuss the different mechanisms by which photon energy can be converted to an electrical current in graphene. Finally, we review applications of graphene as transparent conductive screens, as photodetectors and light modulators at different wavelength ranges.**

***Index Terms*—Graphene, plasmons, photodetectors.**

I. Introduction

GRAPHENE, a single layer of carbon atoms arranged in a hexagonal honeycomb lattice, is the building block of the familiar graphite. Although there are early published reports on graphene [1], it was not until 2004, when Geim and Novoselov at the University of Manchester demonstrated an easy method for isolating graphene [2], that its properties became a subject of intense study [3]–[9]. Graphene is a covalent, π-electron 2-D system with exceptional electrical and optical properties. At low energies, it has a linear dispersion, no bandgap, a high Fermi velocity ($v_F \approx 10^6 \mathrm{ms}^{-1}$), and exhibits very high carrier mobilities [3]–[9]. Unlike conventional metals, its density-of-states and Fermi energy can be tuned by electrostatic or chemical doping. These characteristics have made graphene a prime candidate for applications in nanoelectronics [8], [9]. Graphene also interacts strongly with light, absorbing radiation over a very wide wavelength range extending from the far-infrared (IR) to the ultraviolet [10]–[16]. Interband and intraband single particle excitations, as well as collective plasmon excitations, are supported. The unique combination of outstanding transport properties, wide absorption range, the ability to modulate the absorption [17]–[19], and the short excited state lifetimes [20] have attracted strong interest in its use in photonics and optoelectronics [8], [21]–[23].

Here, we discuss the properties of both single particle and collective excitations of extended graphene and also of confined graphene structures (quantum wires and dots) and their interaction with external fields and the substrate. We discuss the different mechanisms by which light absorption in graphene can generate an electrical current. We briefly review some of the uses of graphene as transparent conductive films for display applications, and in passive optical components, such as polarizers, EM shielding, and saturable absorbers. Then, we discuss applications of graphene and graphene micro- and nanostructures in photodetection and light modulation.

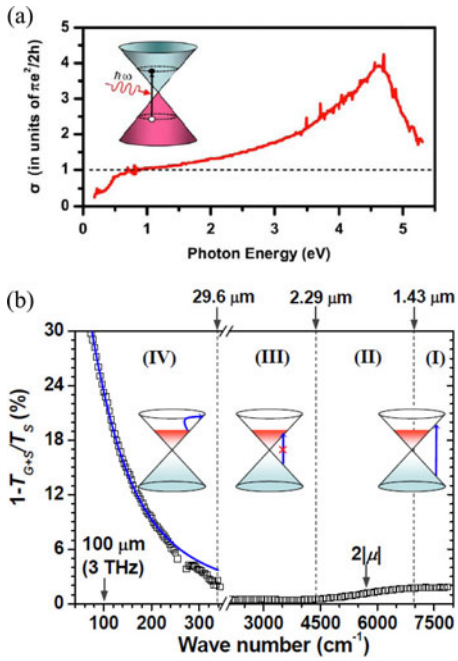

Fig. 1. Optical conductivity of graphene. (a) Optical conductivity of graphene at high photon energies. In the visible range, the optical conductivity is close to the universal value $\pi e^2/2h$. Trigonal warping and many body effects lead to a strong resonance in the UV at 4.6 eV. (Reproduced from [13].) (b) Extinction spectrum of graphene in the IR. ($T_{\mathrm{G+S}}$ is the transmission through graphene and the substrate, T_S is the reference substrate transmission.) Due to Pauli blocking, the absorption drops below the universal value for energies below $2|\mu|$ (twice the chemical potential). In the terahertz range, the absorption increases due to intraband absorption as in metals (Drude peak). However, the Drude weight can be tuned in graphene by electrostatic doping.

II. Optical Properties of Graphene

A. Single Particle Excitations

The optical conductivity of graphene at energies where the dispersion is linear, i.e., in the near-IR and visible, has a universal value given by: $\sigma_{\mathrm{uni}} = \pi e^2/2h$ (see Fig. 1) [10]. Therefore, the absorption of suspended graphene for normally incident light in this frequency range (and $T = 0$) is $A = \pi\alpha \approx 2.3\%$,

Manuscript received April 1, 2013; revised May 23, 2013; accepted June 1, 2013. Date of publication July 31, 2013; date of current version August 14, 2013.

The authors are with IBM T. J. Watson Research Center, Yorktown Heights, NY 10598 USA (e-mail: avouris@us.ibm.com; mfreitag@us.ibm.com).

Color versions of one or more of the figures in this paper are available online at http://ieeexplore.ieee.org.

Digital Object Identifier 10.1109/JSTQE.2013.2272315

where α is the fine structure constant, $e^2/\hbar c$, and c the speed of light [10]. Using a thickness of 0.334 nm for the graphene layer, one obtains an absorption coefficient of about 7×10^5 cm^{-1}, which is about 50 times higher than the absorption of GaAs at 1.55 μm, thus, demonstrating the strong coupling of light and graphene. At the same time, the reflectivity of graphene, *R,* is very low: $R = 0.25\pi^2\alpha^2(1-A) = 1.3 \times 10^{-4}$. At higher photon energies ($\geq$3 eV) the trigonal warping of the bandstructure leads to deviations from the above universal optical conductivity. Many body effects also play an increasingly important role and result in a strong saddle point excitonic resonance near the M point of the Brillouin zone at 4.6 eV; see Fig. 1(a) [13]. The absorption of multilayer graphene is essentially additive, at least at energies above 0.5 eV [10].

A particularly important property of graphene is that it can be doped electrostatically by a gate or chemically by adding dopants. The chemical potential, μ, is determined by the resulting carrier concentration η, $\mu = E_F = \sqrt{\pi\eta}/\hbar$. An important consequence of the Pauli principle and of doping is that interband transitions are essentially blocked for photon energies $\hbar\omega < 2|\mu|$ [Pauli blocking, Fig. 1(b)] [11], [12]. This property provides a way of tuning the absorbance of graphene.

The excited states of graphene produced by photoexcitation or other means decay very fast by different mechanisms. An ultrashort pulse generates electron–hole pairs in a highly nonequilibrium state. Electronic interactions, i.e., Coulombic carrier–carrier interactions such as Auger and impact ionization, which also lead to carrier multiplication, provide the fastest energy redistribution mechanism [24], [25]. Time-resolved fs-scale measurements show that after about 200–300 fs a Fermi–Dirac distribution is attained with an elevated electronic temperature T_e [24], [25]. As expected, the electronic decay rate is a function of the electron density (doping). Along with the energy redistribution processes, energy dissipation takes place via phonon emission. The decay via optical phonons is fast, taking place on a few picosecond time scale [26]. However, when the excitation energy has fallen below the optical phonon energy (about 200 meV), acoustic phonon emission is slow (nanoseconds), and this leads to the formation of an energy dissipation bottleneck [27]. Due to this uncoupling of lattice and electronic temperatures, the resulting "hot" electrons can persist for nanoseconds. Coupling of the electrons with a polar substrate's surface optical phonons may become an important decay path in this case [28].

Optical transitions involving the free electrons of doped graphene lead to absorption that extends into the far-IR and tetrahertz ranges. The optical conductivity in this range has, as in conventional metals, the Drude form [29]:

$$\sigma(\omega) = \frac{iD_{Gr}}{\pi(\omega + i\Gamma)} \tag{1}$$

where the Drude weight, *D,* for graphene has the form [30]: $D_{\mathrm{Gr}} = 2E_F\sigma_{\mathrm{uni}}/\hbar$ and Γ^{-1} is the damping rate. This free electron absorption can, therefore, be made very high, since $\sigma(\omega) \propto E_F \propto \sqrt{\eta}$. Using a gate field, especially using electrolytic gates, carrier densities as high as $\eta \sim 10^{14}$ cm^{-2} can be generated [31]. Also, using heavy chemical doping an increased absorption reaching 40% in a single graphene layer was achieved in the far-IR [32].

Finally, we note that graphene also exemplifies strong nonlinear optical response with an effective nonlinear susceptibility $\left|x^{(3)}\right| \sim 10^{-7}$esu, i.e., approximately eight orders of magnitude larger than in bulk dielectrics [33]. Furthermore, this nonlinearity is essentially dispersionless in the near-IR and visible and has already been utilized in four-wave mixing applications [34], [35] and Kerr effects [36].

B. Collective Excitations—Plasmons

The ever-increasing use of photonics in global data communications and the current interest in on-chip optical communications has led to increased efforts to decrease the physical size and power consumption of photonic devices [37]. One approach involves the use of subdiffraction limit photonic devices based on surface plasmons. In metals–dielectric interfaces, the time-varying electric field associated with the light exerts a force on the metal electron gas and drives it into a collective oscillation, where the restoring force is provided by the resulting gradient of the self-consistent electron field. The light is "bound" to the electrons, its momentum (wave vector) is increased and its apparent wavelength is strongly decreased so that the resulting surface wave (surface plasmon polariton, SPP) provides a strong field localization beyond the diffraction limit, $\lambda_0/2$. The plasmons can be propagating TM or TE waves or localized plasmons in nano- and microparticles [38]. Since at a given frequency ω, the momentum of the plasmon is higher than that of the same frequency light in free space, special techniques, such as prisms or gratings, need to be used to launch the SPP [39]. The field of plasmonics, involving primarily the plasmons of metals (Au, Ag, Cu, Al) and certain other materials, is currently a particularly active field [38], [40]–[42]. The plasmon frequencies of the metals are determined by their electron concentration and the surrounding dielectric, and for noble metals lie generally in the visible and near IR range. Localized plasmon frequencies also depend on the shape of the particles. Graphene support plasmons, but in this case, in the near and far-IR and terahertz ranges (0.1–10 THz). Most importantly, graphene offers the unique capability of plasmon tunability, since, unlike in metals, its charge density can be tuned either by electrostatic or by chemical doping [22], [23], [43]. The plasmon frequency in graphene is given by [43]: $\omega_{\mathrm{pl}}(q) = [(8E_F\sigma_{\mathrm{uni}}k_{\mathrm{pl}})/\hbar\varepsilon]^{1/2}$, where E_F is the Fermi energy, σ_{uni} is the universal conductivity of graphene, k_{pl} is the plasmon momentum, and ε is the dielectric constant of the substrate. Since in graphene $E_F \propto \eta^{1/2}$ it follows that $\omega_{\mathrm{pl}} \propto \eta^{1/4}$ [44], we note that the plasmons of the massless Fermions in graphene are a quantum effect, as is indicated by the presence of $\hbar$ in the aforementioned equation. The compression of the surface plasmon wavelength in graphene λ_{sp} relative to the excitation wavelength λ_0 is strong, and is governed, as is the single particle absorption, by the value of the fine structure constant α [22]. Specifically,

$$\lambda_{\mathrm{sp}}/\lambda_0 \approx (2\alpha E_F/\varepsilon\hbar\omega) \approx \alpha \approx 1/137. \tag{2}$$

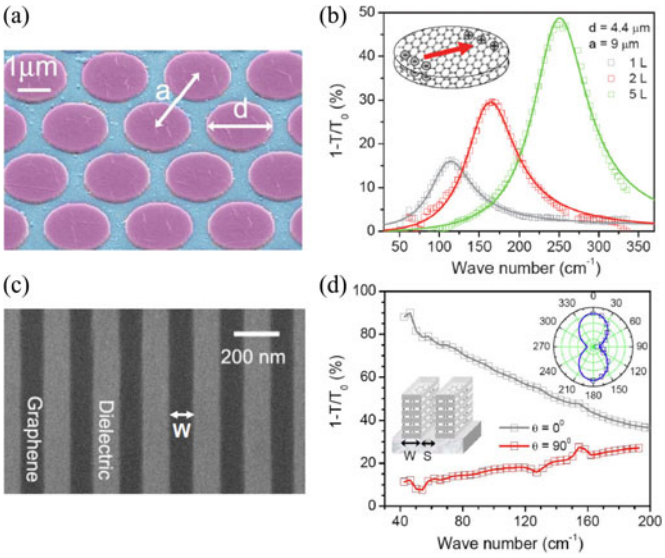

Fig. 2. Standing plasmons in graphene. (a) Image of a graphene microdot array. (b) Extinction spectra of graphene microdot arrays with 1, 2, and 5 graphene layers, separated by polymer buffer layers. The disk diameter was $d = 4.4$ μm, and the triangular lattice constant was $a = 9$ μm. (c) SEM image of a graphene nanoribbon array with 100-nm nanoribbon width. (d) Extinction spectrum of a stacked microribbon array with five graphene layers at 0° and 90° polarization. The ribbon width was 2 μm and the spacing 500 nm. INSET: Polarization dependence of the extinction at 1.2 THz. (Reproduced from [50].)

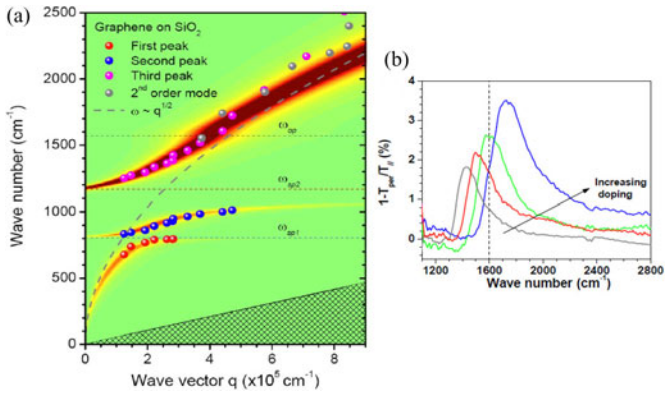

Fig. 3. Dispersion of graphene plasmons on SiO_2. (a) Plasmon dispersion. Three hybrid plasmon–phonon modes are resolved that arise from the interaction of the intrinsic graphene plasmon (dashed curve) with two surface polar phonons of the SiO_2 substrate (sp1 and sp2). Data points are experimental peak positions of plasmons in graphene nanoribbon arrays with different nanoribbon width. The color plot is calculated. (b) Dependence of the third plasmon–phonon peak on chemical doping. The broadening at high doping is due to opening of an additional plasmon decay channel via optical phonons, once the energy exceeds the energy of the graphene optical phonon at 1600 cm^{-1}. (Reproduced from [58].)

For example, for 10 μm incident light, $E_F = 0.15$ eV and a relaxation time of 10^{-13} s, the plasmon wavelength of graphene on SiO_2 will be 155 nm: i.e., a confinement factor λ_0/λ_{sp} of 64. Experimentally, confinement factors of 40–60 have been reported [45], [46]. The confinement normal to the graphene surface is also tight, of the order of $\lambda_{sp}/2\pi$. As a result, field concentrations of the order of 10^6 could develop that can enhance many linear and nonlinear optical phenomena. Another important metric is propagation length (1/e decay of amplitude) δ_{sp} of the surface plasmon determined by the losses in graphene. In perfect graphene samples and energies below the onset of interband transitions and the optical frequency, it could in principle reach $\delta_{sp} \sim 100\lambda_{sp}$ [23]. However, with currently available synthetic graphene samples it will likely be about 3–5 λ_{sp} [47].

Localized plasmons can be excited when the dimension of a micro- or nanostructure is smaller than that of the plasmon, λ_{lp}, which is also a function of the shape of the structure. For example, for a circular disk structure (see Fig. 2) the localized plasmon frequency is given by (3), where d is the disk diameter, and an array of noninteracting circular dots will have an absorption given by (4), where f is the fraction of the graphene surface occupied by the dots [48], [49].

$$\omega_{lp} = \sqrt{\frac{3D}{8\varepsilon_m \varepsilon d}} \tag{3}$$

$$\sigma(\omega) = i\frac{fD}{\pi}\frac{\omega}{(\omega^2 - \omega_p^2) + i\Gamma\omega}. \tag{4}$$

Similarly, localized plasmons with $k = \pi/W$ can be excited in graphene nanoribbons of width W with light perpendicularly polarized to the ribbon axis. The plasmon frequency is now proportional to $1/\sqrt{W}$ [50]. The wavelength compression that takes place upon plasmon excitation in graphene nanoribbons can also be utilized to make very short terahertz antennas that would allow for local communications between microstructures [51], [52]. The plasmons of more complex graphene structures can be described in terms of hybridization of the plasmons of different elementary structures, (disks, rings, etc.), as in the case of metal plasmons [53], [54]. The aforementioned considerations involve structures that are sufficiently separated so as not to interact significantly. Interactions lead to shifts and broadening of the plasmon resonances [50], [55].

The graphene plasmons can interact rather strongly with the substrate. Specifically, polar insulator substrates, such as the commonly used SiO_2, have surface phonons that generate fluctuating electric fields that extend above the substrate surface, and thus, can couple with the plasmons of the supported graphene. As a result, hybrid modes involving collective electronic (plasmon) and ionic lattice (phonon) excitations are generated. The hybrid mode's energy and plasmon content depends on the relative energies and the coupling strengths of the "naked" plasmon and the surface phonons [56], [57]. The hybrid modes have lifetimes that are longer than those of pure plasmons because of the much longer phonon lifetime, which is typically in the picosecond range. Fig. 3 shows the dispersion of graphene plasmon interacting with two surface phonons of SiO_2 [58]. Along with the anticrossing resulting from the interaction of the plasmon with the substrate surface phonon, the effect of coupling with the intrinsic optical phonon of graphene near 200 meV are clearly seen. This coupling with the optical phonon allows the plasmon to decay to electron–hole pairs drastically increasing the damping of the plasmon [58], [59]. The drastic increase in the width of the plasmon as its frequency is increased by chemical doping above the phonon frequency is shown in Fig. 3(b) [58].

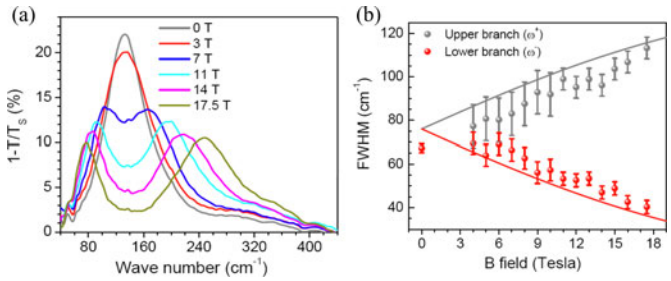

Fig. 4. Magneto-plasmons in graphene. (a) Extinction spectrum of standing graphene plasmons in microdisk arrays of 3 μm diameter for different magnetic field strengths as indicated. The single plasmon peak splits in to two peaks, associated with edge and bulk plasmons. (b) Width of the two magneto-plasmon peaks as a function of magnetic field. The edge-plasmon width is reduced at high magnetic field, indicating a longer life time. (Reproduced from [62].).

Given the interest in the use of patterned graphene in metamaterial structures [60], it is important to consider the losses, i.e., the damping rates, expected in such graphene structures. Taking as an example the graphene nanoribbon (GNR) arrays, we can express the scattering lifetime below the onset of interband transitions (Landau damping) as

$$\tau(q,\omega) \approx [\tau_0^{-1} + \tau_{\text{edge}}(q)^{-1} + \tau_{e-\text{ph}}^{-1}(\omega)^{-1}]^{-1} \tag{5}$$

where τ_0 is lifetime for extended graphene due to scattering by defects. This is approximately the same lifetime as that extracted from the Drude response. For typical synthetic graphene, τ_0 is of the order of 50–100 fs. The edges of graphene introduce additional scattering and $\tau_{\text{edge}}(q)$ has the form $\tau_{\text{edge}}(q) = 2v_F/W_e$, where W_e is the electronic ribbon width and v_F the Fermi velocity [58]. Finally, as we have shown previously, the electron–phonon interaction provides an additional inelastic scattering mechanism, effectively defining the usefulness range of graphene plasmonics to wavelengths below about 6.5 μm (about 50 THz) [58].

C. Magnetoplasmons

At high magnetic field Landau levels are generated in graphene with energies given by [61]:

$$E_n = \pm n v_F \sqrt{2\hbar |eBn|} \tag{6}$$

where n is the Landau level index, B the magnetic field strength, and v_F the Fermi velocity. The cyclotron frequency is given by $\omega_c = eB/m_c$, where m_c is the cyclotron mass, which, unlike the rest mass of graphene, has a finite value dependent on the carrier density. In the cyclotron spectrum, the graphene flake plasmon on a noninteracting substrate, such as a diamond-like carbon film, appears as a single peak whose frequency increases linearly with B. In a graphene microstructure, however, the behavior is more complex. As Fig. 4 shows, with increasing magnetic field strength, the localized plasmon peak in an array of graphene microdisks splits into two peaks which move in opposite directions with increasing field [62]. Their energies are given by

$$\omega^{\pm} = \sqrt{\omega_0^2 + \omega_c^2/4} \pm \omega_c/2. \tag{7}$$

The same behavior is observed at natural inhomogeneities (e.g., step and wrinkles) on graphene surfaces that cause carrier confinement. Futhermore, Faraday rotation spectra show that each peak is excited by a different circular polarization [63]. Most interestingly, the lower energy component becomes narrower, while the higher becomes broader with increasing field. This behavior is related to the quantum Hall effect, but can be qualitatively understood by considering that the plasmon is acted on by the centrifugal forces induced by the magnetic field, which have opposite radial directions for right and left circulating currents in the microdisk, and also by the disk confinement field. Thus, the two interactions can add or subtract from each other. As a result, the zero field plasmon splits into a "bulk" and an "edge" mode in the magnetic field. As the field is increased, the edge plasmon is confined more and more toward the edges of the disks and in effect the 2-D initial plasmon is effectively transformed into a 1-D plasmon, which reduces backscattering, and therefore, also the edge plasmon linewidth [62]. Fig. 4(b) illustrates the changes in the plasmon mode widths as a function of the field strength. More recently, the edge plasmon dynamics in graphene disks were also measured using real time techniques [64]. The dramatic reduction in backscattering in the edge plasmon mode was verified and lifetimes as long as 50 ps (attenuation length $\delta = 70 \pm 30$ mm), i.e., about three orders of magnitude longer than the Drude relaxation time of the sample (0.05 ps for a sample mobility of 5,000 cm^2/Vs), were obtained for the $v = 2$ Landau level. The aforementioned results indicate that magnetic fields provide a powerful way of tuning not only the energy, but also the lifetime of plasmons in graphene.

III. Photocurrent Generation Mechanisms in Graphene

The key process that enables most optoelectronic applications is the conversion of photons into an electrical signal. There are several different mechanisms by which this can be accomplished in graphene. These involve the photovoltaic effect, the photothermoelectric effect, the bolometric effect, and the photon drag effect. In the following, we describe briefly these mechanisms, the situation in which each of them dominates, and their implementation in graphene photodetectors.

A. Photovoltaic Effect

In the photovoltaic effect, the built-in electric fields that are generated at junctions between p- and n-type graphene or between differently doped graphene in general, are employed to separate photogenerated electrons and holes to produce a photocurrent [65]–[67]. A similar result can be achieved through an electric field generated by applying an external bias [68]. If the photogenerated electrons and holes are separated before recombining, they contribute to a photocurrent. Graphene devices fabricated on SiO_2 have been shown to function primarily in the photovoltaic regime [65]–[68]. Opposite doping of two adjacent regions can be achieved with selective chemical doping [69], two (split) gates [65], or by taking advantage of the workfunction difference between graphene and a contacting metal [67]. The split gate and contact geometries are shown in Fig. 5. In the former case, the doping in both regions can be p- or n-type

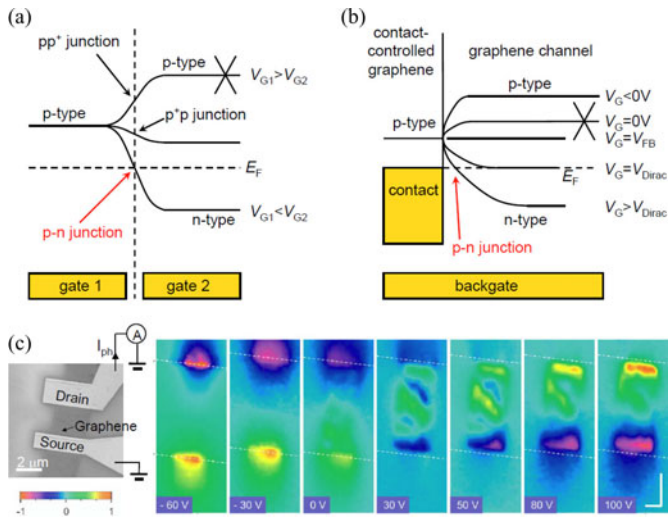

Fig. 5. Photovoltaic effect in graphene. Schematic of the band bending in (a) double-gated graphene p-n junctions, and (b) contacted graphene. (c) Scanning photocurrent images of a graphene field-effect transistor (shown in the gray-scale SEM image) for different backgate voltages as indicated. For negative gate voltages, a pp^+ junction exist right at the contact. At a gate voltage of 30 V, the flat-band voltage is reached and the photocurrent image is dominated by trapped charges in the oxide. For gate voltages in excess of 50 V, p-n junctions are formed about 200 nm away from the contacts. Scale bars on bottom right are both 1 μm. Fig. 5 (c) is reproduced from [67].

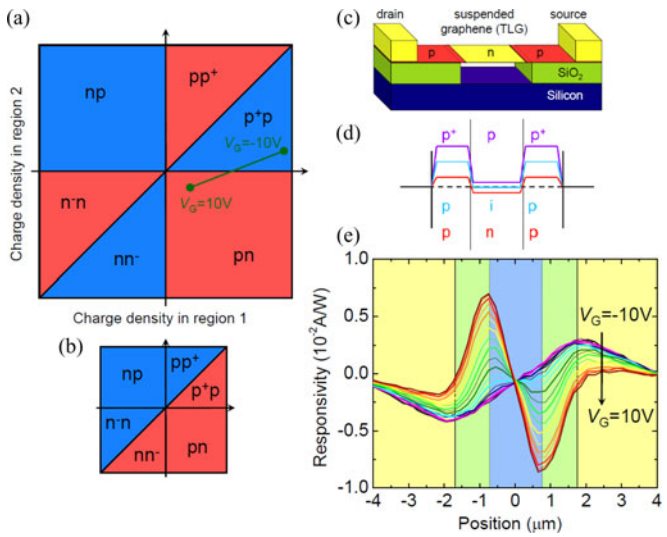

Fig. 6. Thermoelectric current in a suspended graphene p-n junction. (a) Sign of the thermoelectric photocurrent (color coded) as a function of charge density in two adjacent graphene regions. (b) Sign of the photovoltaic photocurrent for comparison. (c) Experimental setup: The supported graphene is doped p-type by the substrate, while the suspended part is close to intrinsic and can be gated n-type by a positive back-gate voltage. (d) Schematic of the band-bending for V_G = –10 V, 0 V, and 10 V (top to bottom). (e) Photocurrent as a function of position along the graphene for different gate voltages as indicated. The photocurrent at the left p-n junction (position -1 μm) switches sign as indicated by the green line in (a). Fig. 6(c) and (e) are reproduced from [76].

depending on the applied gate voltages, while in the latter case, the doping in the contacted area is fixed, typically p-type for high workfunction metals, while the graphene channel can be p- or n-type. The photocurrent direction depends only on the direction of the electric field, not on the overall doping level. Thus, it switches sign, when going from pn to np, or from pp^+ to p^+p. In terms of responsivity of these junction devices, the photocurrent usually peaks around 10^{-2} or 10^{-3} A/W.

The speed with which these photovoltaic photodetectors can be operated has been measured by several groups [70]–[72]. Bandwidth values up to 500 GHz have been reported in these references. Note that energy loss through electron–electron scattering is beneficial in terms of efficiency, since it effectively increases the number of carriers with excess energy that have a chance of contributing to a photocurrent. Electron–phonon scattering, on the other hand, transfers energy from the electron system to the phonon system, which may produce bolometric effects such as will be discussed in Section III-C, but does not lead to carrier multiplication. In graphene, the Dirac electron structure and efficient electron–electron scattering means that photogenerated carriers will multiply rapidly and share their excess energy with the electron bath, while electron–acoustic phonon scattering is weak, so further thermalization is limited. This effectively produces an elevated electron temperature T_e above the lattice temperature increase $T_{\rm ph}$. In traditional optically active materials, hot electron operation requires very low temperatures, which reduces electron–phonon coupling.

B. Photothermoelectric Effect

An optically generated gradient $dT_{\rm e}/dx$ in the electron temperature $T_{\rm e}$, together with a spatially varying Seebeck coefficient such as in p-n junctions, may produce a photocurrent due to the thermoelectric effect (see Fig. 6). This effect has been shown to dominate in graphene p-n junctions with atomically flat boron-nitride dielectrics [73]–[75] or in suspended graphene [76]. Because hot electrons rather than lattice heating generate the electronic response in these references, photothermoelectric graphene detectors could show similarly high bandwidth as in the photovoltaic case. The thermoelectric current is proportional to $(S_2 - S_1)\, dT_{\rm e}/dx$, where S_1 and S_2 are the Seebeck coefficients of the p- and n-type regions. The Seebeck coefficients are related to the electrical conductivity σ through the Mott formula $S = -\frac{\pi^2 k_{\rm B}^2 T_{\rm e}}{3e} \frac{1}{\sigma} \frac{d\sigma}{d\varepsilon}$, and thus, they can be calculated from the $I-V_G$ characteristic. In contrast to the photovoltaic current discussed previously, the thermoelectric current shows sign reversal in bipolar p-n junctions on the one hand, and unipolar p^+p or nn^- junctions on the other. This is due to the sign change of the transconductance $d\sigma/d\varepsilon$ when going from p-type transport to n-type transport. Together with the sign reversal when switching the electric field direction, this leads to a six-fold sign change in the photocurrent as a function of the doping in the two regions [see Fig. 6(a) and (b)]. This behavior can be used to differentiate between photovoltaic and photothermoelectric effects [74].

Typical responsivities on the order of 10^{-3} A/W have been reported for the photothermoelectric effect in graphene similar to the ones observed in photovoltaic graphene photodetectors. However, particularly high responsivities on the order of 10^{-2} A/W have been measured in suspended graphene p-n junctions [see Fig. 6(e)] [76]. In these, the interaction of substrate phonons with graphene electrons is prohibited in the suspended

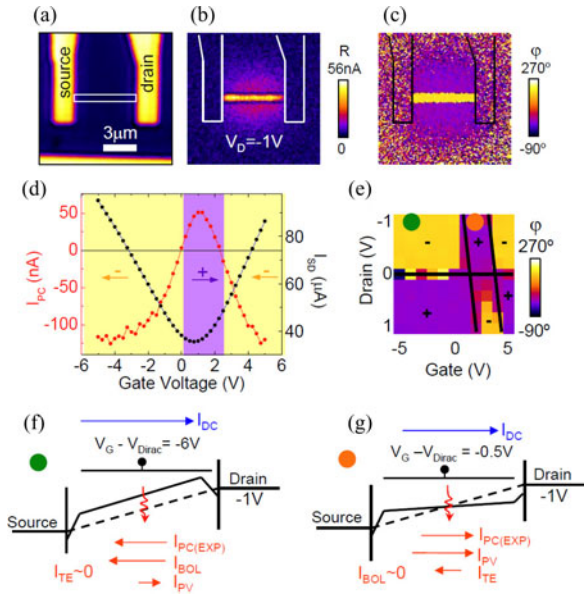

Fig. 7. Bolometric (BOL) and Photovoltaic (PV) components of the photocurrent in biased graphene transistors. (a) Reflected light image of the device. (b) Photocurrent amplitude and (c) phase as a function of position in a biased device. ($\lambda = 690$ nm laser wavelength, $P = 220$ μW laser power, gate voltage $V_G = 5$ V.) (d) Transport current and photocurrent as a function of gate voltage. (Drain voltage $V_D = -1$ V; laser power $P = 370$ μW.) The photocurrent is positive near the Dirac point due to the PV effect and negative elsewhere due to the BOL effect. (e) Photocurrent sign as a function of drain and gate voltage. Schematic of the band bending in the doped (f, green) and intrinsic (g, orange) cases. PC (EXP): experimental photocurrent; TE: thermoelectric photocurrent. Reproduced from [68].

part, removing a potential electron–phonon decay channel. This shows that electron/substrate polar phonon scattering can be the dominating electron–phonon decay channel, especially at room temperature, and removing it by suspending, therefore, increases the hot electron temperature and photocurrent.

C. Bolometric Effect

The bolometric effect is defined as a change in transport current due to the heating associated with the incident photons. It thus requires an externally applied bias, and homogeneous graphene is used instead of p-n junctions. The transport current is altered by incident light in two main ways: the current can change due to changes in carrier mobility with temperature, or the current can change due to the presence of additional photocarriers. The latter is simply the photovoltaic effect, with the electric field generated by the external bias. If electrons and lattice are equilibrated after photoexcitation, these effects can be lumped together by considering simply the temperature dependence of the resistivity $R(T)$. In the case of graphene, since $T_e > T_{ph}$, the two mechanisms have to be treated separately, and in [68], it was shown that the two mechanisms have opposite photocurrent sign in graphene (see Fig. 7). The excess carriers lead to a current in the direction of the transport current, while the temperature dependence of the mobility leads to a negative photocurrent. It is important to note that by changing the Fermi level in graphene, one can choose which mechanism dominates [see Fig. 7(d) and (g)]. Near the Dirac point, where the carrier density is lowest, the effect of the additional photocarriers is greatest, while far away from the Dirac point the mobility reduction dominates.

As a function of both drain and gate bias, a six-fold sign change is observed [Fig. 7(e)] reminiscent of the six-fold sign change observed for the thermoelectric effect in double-gated graphene p-n junctions [Fig. 6(a)]. Here, however, the thermoelectric effect is weak due to the homogeneity of graphene in the channel. The six-fold sign change instead is brought about by the interplay of photovoltaic and bolometric effects with opposite sign. Of course, there could also be a thermoelectric effect present, since the Seebeck coefficient changes due to a slight doping gradient induced by the bias. However, this effect should be strongest near the Dirac point and have a negative sign there, which is opposite of what was observed in Fig. 7. In [68], the elevated electron and lattice temperatures were calculated from the photovoltaic and bolometric components of the photocurrent. It was found that the electron temperature is indeed increased compared to the lattice temperature by an order of magnitude, and that the differences are highest near the Dirac point.

D. Phonon Drag Effect

Yet another way to induce a photocurrent in graphene without applying a bias is provided by the photon drag effect. This is a second-order effect that utilizes the transfer of momentum by incident photons to impart momentum to free carriers via electron–phonon coupling. The effect depends on the polarization and incidence angle of the photons and it has been first demonstrated in nanographite [77]. By this mechanism ultrafast currents can be launched in graphene.

IV. Device Implementations

A. Transparent Conductive Films and Passive Photonic Devices

The high conductivity, mechanical flexibility, and optical transparency of graphene are widely expected to find a range of applications, including LEDs and OLEDs, solar cells, touchscreens, smart windows, and LCD films [78]–[84]. Currently, the material used in most of these applications is ITO which has a transmittance of ~90% and a sheet resistance between 10–50 Ωsq^{-1}. ITO, however, is both expensive and brittle and graphene is considered as a possible alternative. Different applications require different properties from the graphene films. A typical undoped graphene layer has a sheet conductivity of about 500 Ωsq^{-1}. Most applications, on the other hand, require much higher conductivities. For example, solar cells and OLED displays require resistances less than ~50 Ωsq^{-1}, while touch screens are more forgiving [79]. The conductance of graphene can be increased by external doping with agents such as HNO_3 and $AuCl_3$, although the long-term stability of this type of doping is currently a problem. The large area graphene needed for these window/display types of applications must come from CVD, since graphene from SiC is limited by the size of available SiC wafers and is prohibitively expensive. The large area CVD graphene has to be transferred from the metal catalyst (usually

copper) surface to the appropriate substrate without tearing or wrinkling. This offers a big challenge, but significant efforts are made to achieve roll-to-roll transfer by companies such as Samsung [78] and Sony [85].

The high absorption of doped graphene in the microwave and terahertz regions can be used as an effective shield for EM radiation. Traditionally, materials such as ferrite or metal nanocomposites are employed for that purpose and millimeter thicknesses of these materials are needed for effective shielding [86], [87]. Graphene, on the other hand, is ~1,000 times thinner, light, flexible and strong, and only about five layers are needed to produce a >20 dB shielding efficiency [32].

Two different types of polarizers based on graphene have been demonstrated. One is an in-line fiber polarizer, which relies on polarization-selective coupling between the evanescent field and graphene [88]. The authors demonstrated that the out-coupled light in the telecommunication band shows a strong s-polarization effect with an extinction ratio of 27 dB. The other is based on graphene nanoribbon arrays, where the light can couple to the localized plasmons of the ribbon only when polarized perpendicular to the ribbon axis [50].

Another application of graphene is as a saturable absorber. Saturable absorption describes the condition where the absorption of light by a material decreases with increasing light intensity. Most materials show saturable absorption, but often only at very high optical intensities, close to the optical breakdown threshold. Saturable absorbers are used in laser cavities for mode-locking and Q-switching. Graphene with its wide absorption range, fast decay and high stability is well suited for this application in the IR, and indeed has been successfully used to produce picosecond laser pulses [89]–[92].

B. Optical Modulators

The ability to modulate the Fermi level of graphene by a gate field naturally leads to its application as a fast electro-absorption modulator. High speed, small footprint, and high bandwidth modulators are highly desirable for optical communications. However, although the light–graphene interaction is strong, the extent of absorption of a light beam by a single graphene layer is insufficient. For this purpose, the graphene was coupled with a silicon waveguide to increase the absorption, and a modulation by 0.1 dBμm^{-1} of the guided light (1.35 to 1.6 μm) at frequencies over 1 GHz was demonstrated (see Fig. 8) [93]. An alternative modulator design involving two layers of graphene, separated by a thin dielectric on top of the silicon waveguide, has also been successfully demonstrated [94]. A different approach to electro-optic modulation involved the modulation of a photonic crystal nanocavity by an electrically gated graphene layer. By tuning the Fermi level of graphene, one can modulate the reflectivity of the cavity at telecom wavelengths by more than 10 dB [95]. Graphene-based modulators operating in the terahertz range have also been proposed [96].

C. Photodetectors

Silicon, germanium, or compound semiconductors like InGaAs have traditionally been used for photodetection, particularly in optical communications. More recently, optical interconnects were also investigated as alternatives to electrical wiring in ultrahigh bandwidth intra- and interchip links. In this respect, it is important to be able to integrate the silicon CMOS technology and photonic devices on a single chip. Graphene is compatible with the silicon technology and this, in conjunction with its unique optical and electrical properties, have resulted in an intense effort to utilize graphene for these critical photonic functions.

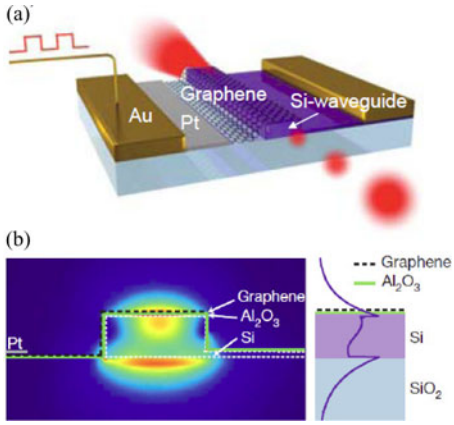

Fig. 8. Optical modulator. (a) Schematic of an optical modulator based on a silicon waveguide and graphene absorber. The graphene is contacted by the left Au/Pd electrode, while the silicon waveguide is contacted through a thin layer of silicon by the right electrode. Graphene is separated from the silicon by a thin layer of aluminum-oxide. A bias between graphene and silicon is used to electrostatically dope the graphene. Optical modulation by 0.1 dBμm^{-1} of the guided light (1.35 to 1.6 μm) was demonstrated with a swing voltage of a few volts. (b) Cross section through the device and mode profile of the single-mode waveguide. The mode was designed to maximize the electric field at the position of the graphene. (Reproduced from [93].)

The first demonstration of a graphene photodetector was based on a metal–graphene contact. In that case, a graphene–metal junction was irradiated by light in the IR and visible parts of the spectrum [72]. Fig. 9 shows the measured ac photoresponse of a single metal (Pd)–graphene junction to a 1.55 μm intensity modulated light beam. A nearly constant response was observed up to 40 GHz, which was the upper frequency limit of the measurement system used. Modeling, however, suggested that eventually the detector response of such devices will be limited by their RC constant to about 0.6 THz [72]. In such a symmetric junction device, simultaneous illumination of both opposite contact regions would produce equal but opposite polarity currents, and therefore, no net photocurrent. An improved design shown in Fig. 9(b) provided a significantly increased photoresponsivity (photocurrent/input optical power) and allowed one to utilize the full surface of the device for photodetection [97]. This device utilized interdigitated metal electrodes made of two different metals, one with a high work function (e.g., Pd) and the other with a low work function (e.g., Ti). These two different work functions produced different doping and band-bending in graphene that allowed photodetection over the entire area of the device. This device was used to test its suitability in optical communications. It was shown that it could reliably detect optical data streams of 1.55 μm light pulses at the highest available rate of 10 GBits/s [97].

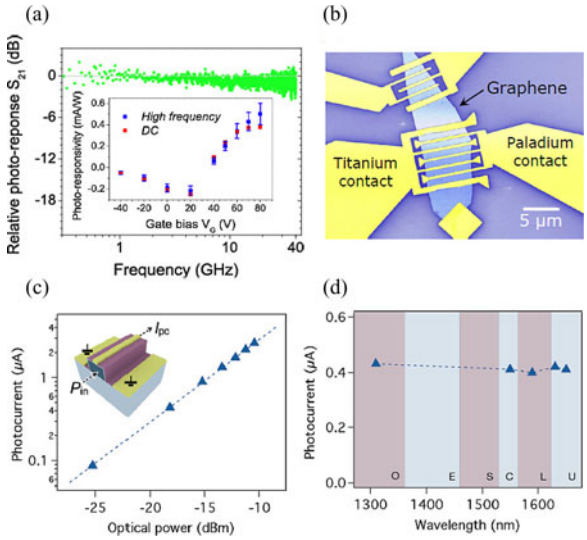

Fig. 9. Graphene photodetectors. (a) High-speed graphene photodetector measured up to 40 GHz with no degradation in signal level. The IR light at 1.55μm wavelength was focused onto a graphene–metal contact. (b) Graphene photodetector design optimized for collection over larger areas by utilizing interdigitated finger electrodes with different metal composition. (c) Enhanced photoresponse due to integration of a graphene photodetector with a silicon waveguide. The main figure shows the photocurrent versus optical power injected into the waveguide. Inset: detector layout using one centrally located signal electrode and two grounded electrodes contacting graphene. (d) Remarkable uniformity in photocurrent over different telecommunication bands for the device in (c). (Reproduced from [72], [97], and [100].)

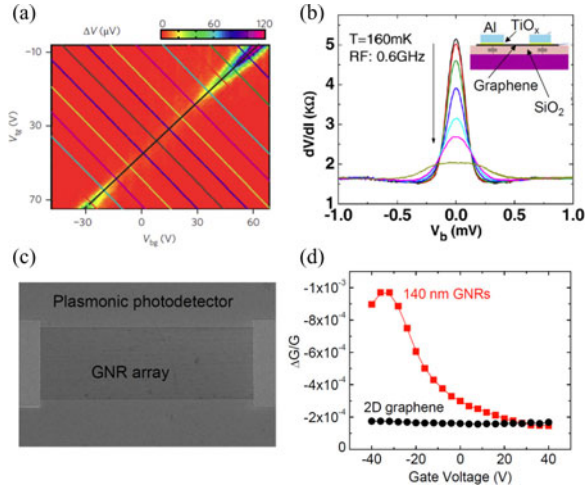

Fig. 10. Graphene bolometers. (a) Dual-gated bilayer graphene hot-electron bolometer. The plot shows the photoresponse as a function of top and bottom gate voltages. The device was dc biased at 255 nA and the temperature was 6 K. Along the diagonal, the Fermi level is balanced at charge neutrality. In this range, the photoresponse increases strongly for increasing perpendicular electric field due to opening of a bandgap in bilayer graphene. (b) Bolometer based on tunnel junctions between graphene and superconducting aluminum with thin TiO_x tunneling barrier. The plot shows the dynamic resistance as a function of bias voltage for increasing radio-frequency power. The graphene acts as the absorber, whereas the tunneling junction, cooled below the critical temperature of aluminum, acts as the temperature-sensitive element. (c) SEM image of a plasmonic photodetector utilizing a graphene nanoribbon array. (d) Normalized conductance change as a function of gate voltage. The 140-nm GRN array shows a strong plasmonic enhancement for light at 10.6 μm and polarization perpendicular to the GNRs. The response is gate-voltage tunable. (Reproduced from [106], [109], and [57].)

To further increase the photoresponse, graphene can be incorporated inside Fabry–Pérot microcavities. In one case two semitransparent metallic mirrors were utilized to form the resonant cavity and the graphene was placed at the position of the maximum field leading to a 20-fold enhancement of the photocurrent at the resonant wavelength [98]. Another study utilized Bragg reflectors and achieved 60% absorption at a resonance wavelength of 850 nm [99]. The most recent study [100] [see Fig. 9(c) and (d)] combined graphene with a silicon waveguide to both enhance the responsivity of graphene and also to demonstrate the ability to integrate with silicon (this approach has also been utilized in the case of light modulators discussed previously). In this way, the authors demonstrated photodetection with a responsivity of 0.03–0.05 AW^{-1} over all fiber-optic communication bands, from O- to U-band, that is beyond the 1605-nm wavelength range of strained germanium photodetectors [101] and with a much smaller footprint than ion-implanted Si detectors [102].

Other approaches to further increase the response of graphene photodetectors involved a combination of graphene and other photoactive materials. Charge transfer between the photoexcited material and graphene leads to residual opposite charges on that material and amplification due to the graphene transistor action. For example, by decorating graphene with gold nanoparticles and exciting in the visible the plasmonic resonances of the nanoparticles, a large plasmonic field enhancement was obtained [103]. This is the same effect that leads to the giant enhancement of the Raman spectra by such localized plasmon resonances. A disadvantage of this approach is that the excitation/detection wavelength is now determined by the resonance of the nanoparticle not graphene. A similar approach involved sandwiching gold nanoantennas (heptamer gold particle arrays) between two layers of graphene. The photocurrent was enhanced both by the field enhancement and by hot electron injection leading up to a 20% internal quantum efficiency [104]. Semiconductor nanoparticle (PbS) arrays on graphene have also been utilized to enhance photodetection. Photoexcitation of the nanoparticle lead to charge transfer to graphene, a large enhancement of the device capacitance, and a huge, 10^8, gain [105]. The large RC, however, limits the speed of the device and the narrow spectrum of the nanoparticle, the operating wavelength.

Since electrons in graphene are coupled very weakly to the thermal bath, and thermalization within the electron gas is very fast, the bolometric effect is of particular interest (see Section III-C). However, since graphene does not have a bandgap, the temperature dependence of its resistivity is generally weak. Fortunately, there are several approaches that could make the basic bolometric response much more sensitive. It has, for example, been shown that gapped bilayer graphene can have advantages over single-layer graphene [see Fig. 10(a)] [106]. Applying an electric field perpendicular to the graphene sheets opened a bandgap in Bernal-stacked bilayer graphene [107], [108]. The increased resistance and temperature-dependence of resistance lead to higher responsivity and a very low noise equivalent power (33 fW $Hz^{-1}/2$ at 5 K) [106]. Another approach of providing large temperature dependence and low noise equivalent power is the utilization of superconducting leads in combination with tunnel junctions between graphene and the lead [see

Fig. 10(b)] [109]. This approach makes use of the superconducting gap of the contacts with high temperature dependence around the critical temperature T_C, rather than the temperature dependence of the graphene itself. In this case, graphene acts as the absorber and heat conductor, while the superconducting tunnel junctions act as the active elements. Finally, Johnson noise thermometry on single-layer graphene contacted by regular metals, may also be a viable approach for ultrasensitive graphene bolometry [110].

A photodetection scheme based on plasmonics of graphene, patterned into metamaterials structures such as nanoribbons, was proposed recently [see Fig. 10(c) and (d)] [57]. As we discussed in Section II-B, GNRs exhibit well defined, width-dependent plasmonic resonances that can be excited by s-polarized light. The basis of this approach is to use the excitation of the *intrinsic* plasmons of the nanoribbons to enhance the photoresponsitivity of the detector. Moreover, because of the dual tunability provided by choosing the width of the nanoribbon and the gate dependent tuning of the plasmon resonance, the detector can be made frequency selective for frequencies in the IR and terahertz ranges [57]. Due to the interaction of GNR plasmon with surface phonon polaritons of the SiO_2 substrate these resonances are hybrids of the two types of excitations. In the implementation of this approach, arrays of nanoribbon with widths ranging between 80 and 200 nm were fabricated lithographically. Their plasmon resonances were then tuned by gate modulation of the chemical potential to be brought successively in coincidence with the frequency of the exciting beam, in this case, a CO_2 laser beam at 943 cm^{-1}. The resulting photocurrent was measured with both s- and p-light polarization to determine the effect of plasmon versus interband (electron–hole) excitation. Indeed, an order of magnitude higher photocurrent and a four-fold increase in temperature was observed for s-polarization. Interestingly, the sign of the photocurrent itself was found to be polarization sensitive in narrow GNRs, and this was interpreted in terms of a competition of the decay of the resulting excitation into electron–hole pairs or phonons [57].

Photodetection using graphene can be extended all the way to terahertz frequencies. Indeed, Vicarelli *et al.* [111] have demonstrated top-gated graphene FETs that exploit the nonlinear response of the gate electrode to the terahertz oscillating field to produce a dc signal proportional to the optical power. In this way, they detected 0.3-THz radiation at room temperature. Log-periodic, circular-toothed antennas were used for the gate and source electrodes and a metal line for the drain electrode.

The possibility of generating terahertz radiation using graphene has also been explored. Early on the use of graphene as a gain medium for stimulated emission by optical pumping was proposed [112]. Experimental studies on graphene and multilayer graphene using a pulsed fs laser did lead to terahertz emission [113], which, however, is 10^3–10^4 times weaker that produced by III–IV devices [114].

V. Conclusion

Graphene is the ultimate thin 2-D material, with a strong interaction with light over a very wide wavelength range. The wide absorption of graphene coupled with its excellent conductivity, mechanical strength, lightness, flexibility and compatibility with silicon technology make an ideal candidate for photonic and optoelectronic applications. Although the light absorption of graphene via interband excitations is strong, for a single atomic layer, it is not sufficient for most photonic applications. However, as we have seen, integration with silicon waveguides or in photonic cavities can significantly enhance the absorption, allowing graphene to be utilized in a variety of photonic functions such as light guiding, routing, and light modulation and detection. In the far-IR and tetrahertz frequency ranges, light absorption in graphene involves intraband transitions whose strength can be large and tunable by electrostatic or tunable doping. Just a few layers of graphene provide sufficient absorption. By coupling to graphene localized plasmons the light–graphene interaction can be further enhanced and wavelength-selective absorption is possible. Graphene plasmonics may enable, besides transparent and conductive screens, detectors and modulators, other applications such as terahertz communications, mid- and far-IR imaging and spectroscopy. This is just the beginning of the exploration of graphene in photonics and is to be expected that many innovations will result from future studies of this fascinating material.

Acknowledgment

The authors would like to thank their coworkers H. Yan, F. Xia, T. Low, T. Mueller, W. Zhu, V. Perebeinos, and Z. Li for all their contributions to the work described here and many valuable discussions.

References

[1] P. Avouris, "Graphene: Electronic and photonic properties and devices," *Nano Lett.*, vol. 10, pp. 4285–4294, 2010.

[2] K. S. Novoselov, A. K. Geim, S. V. Morozov, D. Jiang, Y. Zhang, S. V. Dubonos, I. V. Grigorieva, and A. A. Firsov,, "Electric field effect in atomically thin carbon films," *Sci.*, vol. 36, pp. 666–669, 2004.

[3] C. Berger, Z. Song, T. Li, X. Li, A. Y. Ogbazghi, R. Feng, Z. Dai, A. N. Marchenkov, E. H. Conrad, P. N. First, and W. A. de Heer,, "Ultrathin epitaxial graphite: 2d electron gas properties and a route toward graphene-based nanoelectronics," *J. Phys. Chem. B*, vol. 108, pp. 19912–19916, 2004.

[4] Y. Zhang, Y. Tan, H. L. Stormer,, and P. Kim, "Experimental observation of the quantum Hall effect and Berry's phase in graphene," *Nature*, vol. 438, pp. 201–204, 2005.

[5] A. H. Castro Neto, F. Guinea, N. M. R. Peres, K. S. Novoselov, and A. K. Geim,, "The electronic properties of graphene," *Rev. Mod. Phys.*, vol. 81, pp. 109–162, 2009.

[6] A. K. Geim and K. S. Novoselov,, "The rise of graphene," *Nat. Mater.*, vol. 6, pp. 183–191, 2007.

[7] P. N. First, W. A. de Heer, T. Seyller, C. Berger, J. A. Stroscio, and J. S. Moon,, "Epitaxial graphenes on silicon carbide," *MRS Bull.*, vol. 35, pp. 296–305, 2010.

[8] P. Avouris and F. Xia,, "Graphene applications in electronics and photonics," *MRS Bull.*, vol. 37, pp. 1225–1234, 2012.

[9] P. Avouris and C. Dimitrakopoulos,, "Graphene: Synthesis and applications," *Mater. Today*, vol. 15, pp. 86–97, 2012.

[10] R. R. Nair, P. Blake, A. N. Grigorenko, K. S. Novoselov, T. J. Booth, T. Stauber, N. M. R. Peres, and A. K. Geim,, "Fine structure constant defines visual transparency of graphene," *Science*, vol. 320, pp. 1308, 2008.

[11] A. B. Kuzmenko, E. van Heumen, F. Carbone, and D. van der Marel,, "Universal optical conductance of graphite," *Phys. Rev. Lett.*, vol. 100, p. 117401, 2008.

[12] K. F. Mak, M. Y. Sfeir, Y. Wu, C. Lui, J. A. Misewich, and T. F. Heinz,, "Measurement of the optical conductivity of graphene," *Phys. Rev. Lett.*, vol. 101, p. 196405, 2008.

[13] K. F. Mak, J. Shan, and T. F. Heinz, "Seeing many-body effects in single- and few-layer graphene: Observation of two-dimensional saddle-point excitons," *Phys. Rev. Lett.*, vol. 106, pp. 046401-1–046401-4, 2011.

[14] L. A. Falkovsky and S. S. Pershoguba, "Optical far-infrared properties of a graphene monolayer and multilayer," *Phys. Rev. B*, vol. 76, p. 153410, 2007.

[15] J. M. Dawlaty, S. Shivaraman, J. Strait, P. George, M. Chandrashekhar, F. Rana, M. G. Spencer, D. Veksler, and Y. Chen, "Measurement of the optical absorption spectra of epitaxial graphene from terahertz to visible," *Appl. Phys. Lett.*, vol. 93, pp. 131905-1–131905-3, 2008.

[16] M. Orlita and M. Potemski, "Dirac electronic states in graphene systems: Optical spectroscopy studies," *Semicond. Sci. Tech.*, vol. 25, pp. 063001–063022, 2010.

[17] Z. Q. Li, E. A. Henriksen, Z. Jiang, Z. Hao, M. C. Martin, P. Kim, H. L. Stormer, and D. N. Basov, "Dirac charge dynamics in graphene by infrared spectroscopy," *Nat. Phys.*, vol. 4, pp. 532–535, 2008.

[18] F. Wang, Y. Zhang, C. Tian, C. Girit, A. Zettl, M. Crommie, and Y. R. Shen,, "Gate-variable optical transitions in graphene," *Science*, vol. 320, pp. 206–209, 2008.

[19] F. T. Vasko and V. Ryzhii,, "Voltage and temperature dependencies of conductivity in gated graphene," *Phys. Rev. B*, vol. 76, p. 233404, 2007.

[20] D. Sun, Z.-K. Wu, C. Divin, X. Li, C. Berger, W. A. de Heer, P. N. First, and T. B. Norris, "Ultrafast relaxation of excited dirac fermions in epitaxial graphene using optical differential transmission spectroscopy," *Phys. Rev. Lett.*, vol. 101, p. 157402, 2008.

[21] F. Bonaccorso, Z. Sun, T. Hasan, and A. C. Ferrari, "Graphene photonics and optoelectronics," *Nat. Photon.*, vol. 4, pp. 611–622, 2010.

[22] A. N. Grigorenko, M. Polini, and K. S. Novoselov, "Graphene plasmonics," *Nat. Photon.*, vol. 6, pp. 749–758, 2012.

[23] Q. Bao and K. P. Loh, "Graphene photonics, plasmonics, and broadband optoelectronic devices," *ACS Nano*, vol. 6, pp. 3677–3694, 2012.

[24] E. Malic, T. Winzer, E. Bobkin, and A. Knorr, "Microscopic theory of absorption and ultrafast many-particle kinetics in graphene," *Phys. Rev. B*, vol. 84, p. 205406, 2011.

[25] R. Kim, V. Perebeinos, and P. Avouris, "Relaxation of optically excited carriers in graphene," *Phys. Rev. B*, vol. 84, p. 075449, 2011.

[26] H. Wang, J. H. Strait, P. A. George, S. Shivaraman, V. B. Shields, M. Chandrashekhar, J. C. M. Hwang, F. Rana, M. G. Spencer, C. S. Ruiz-Vargas, and J. Park, "Ultrafast relaxation dynamics of hot optical phonons in graphene," *Appl. Phys. Lett.*, vol. 96, p. 081917, 2010.

[27] R. Bistritzer and A. H. MacDonald, "Electronic cooling in graphene," *Phys. Rev. Lett.*, vol. 102, p. 206410, 2009.

[28] T. Low, V. Perebeinos, R. Kim, M. Freitag, and P. Avouris, "Cooling of photoexcited carriers in graphene by internal and substrate phonons," *Phys. Rev. B*, vol. 86, p. 045413, 2012.

[29] C. Kittel, *Introduction to Solid State Physics*. Hoboken, NJ, USA: Wiley, 2005.

[30] Y. Zheng and T. Ando, "Hall conductivity of a two-dimensional graphite system," *Phys. Rev. B*, vol. 65, p. 245420, 2002.

[31] D. K. Efetov and P. Kim, "Controlling electron-phonon interactions in graphene at ultrahigh carrier densities," *Phys. Rev. Lett.*, vol. 105, p. 256805, 2010.

[32] H. Yan, F. Xia, W. Zhu, M. Freitag, C. Dimitrakopoulos, A. A. Bol, G. Tulevski, and P. Avouris, "Infrared spectroscopy of wafer-scale graphene," *ACS Nano*, vol. 5, pp. 9854–9860, 2011.

[33] E. Hendry, P. J. Hale, J. Moger, A. K. Savchenko, and S. A. Mikhailov, "Coherent nonlinear optical response of graphene," *Phys. Rev. Lett.*, vol. 105, p. 097401, 2010.

[34] Z. Zhang and P. L. Voss, "Full-band quantum-dynamical theory of saturation and four-wave mixing in graphene," *Opt. Lett.*, vol. 36, pp. 4569–4571, 2011.

[35] T. Gu, N. Petrone, J. F. McMillan, A. van der Zande, M. Yu, G. Q. Lo, D. L. Kwong, J. Hone, and C. W. Wong, "Regenerative oscillation and four-wave mixing in graphene optoelectronics," *Nat. Photon.*, vol. 6, pp. 554–559, 2012.

[36] H. Zhang, S. Virally, Q. L. Bao, K. P. Loh, S. Massar, N. Godbout, and P. Kockaert, "Large nonlinear kerr effect in graphene," *arXiv:1203.5527*, 2012.

[37] R. Kirchain and L. Kimerling, "A roadmap for nanophotonics," *Nat. Photon.*, vol. 1, pp. 303–305, 2007.

[38] S. Maier, *Plasmonics: Fundamentals and Applications*. New York, NY, USA: Springer, 2007.

[39] A. V. Zayats, I. I. Smolyaninov, and A. A. Maradudin, "Nano-optics of surface plasmon polaritons," *Phys. Rep.*, vol. 408, pp. 131–314, 2005.

[40] M. W. Knight, H. Sobhani, P. Nordlander, and N. J. Halas, "Photodetection with active optical antennas," *Science*, vol. 332, pp. 702–704, 2011.

[41] A. Boltasseva and H. A. Atwater, "Low-Loss plasmonic metamaterials," *Science*, vol. 331, pp. 290–291, 2011.

[42] P. R. West, S. Ishii, G. V. Naik, N. K. Emani, V. M. Shalaev, and A. Boltasseva, "Searching for better plasmonic materials," *Laser Photon. Rev.*, vol. 4, pp. 795–808, 2010.

[43] F. H. L. Koppens, D. E. Chang, and F. Javier Garcia de Abajo,, "Graphene plasmonics: A platform for strong lightmatter interactions," *Nano Lett.*, vol. 11, pp. 3370–3377, 2011.

[44] E. H. Hwang and S. Das Sarma, "Dielectric function, screening, and plasmons in two-dimensional graphene," *Phys. Rev. B*, vol. 75, p. 205418, 2007.

[45] Z. Fei, A. S. Rodin, G. O. Andreev, W. Bao, A. S. McLeod, M. Wagner, L. M. Zhang, Z. Zhao, M. Thiemens, G. Dominguez, M. M. Fogler, A. H. C. Neto, C. N. Lau, F. Keilmann, and D. N. Basov, "Gate-tuning of graphene plasmons revealed by infrared nano-imaging," *Nature*, vol. 487, pp. 82–85, 2012.

[46] J. Chen, M. Badioli, P. Alonso-Gonzalez, S. Thongrattanasiri, F. Huth, J. Osmond, M. Spasenovic, A. Centeno, A. Pesquera, P. Godignon, A. Zurutuza Elorza, N. Camara, F. J. G. de Abajo, R. Hillenbrand, and F. H. L. Koppens, "Optical nano-imaging of gate-tunable graphene plasmons," *Nature*, vol. 487, pp. 77–81, 2012.

[47] P. Tassin, T. Koschny, M. Kafesaki, and C. M. Soukoulis, "A comparison of graphene, superconductors and metals as conductors for metamaterials and plasmonics," *Nat. Photon.*, vol. 6, pp. 259–264, 2012.

[48] S. J. Allen, H. L. Stormer, and J. C. M. Hwang, "Dimensional resonance of the two-dimensional electron gas in selectively doped GaAs/AlGaAs heterostructures," *Phys. Rev. B*, vol. 28, p. 4875, 1983.

[49] R. P. Leavitt and J. W. Little, "Absorption and emission of radiation by plasmons in two-dimensional electron-gas disks," *Phys. Rev. B*, vol. 34, pp. 2450–2457, 1986.

[50] H. Yan, X. Li, B. Chandra, G. Tulevski, Y. Wu, M. Freitag, W. Zhu, P. Avouris, and F. Xia, "Tunable infrared plasmonic devices using graphene/insulator stacks," *Nat. Nanotechnol.*, vol. 7, pp. 330–334, 2012.

[51] I. F. Akyildiz and J. M. Jornet, "Electromagnetic wireless nanosensor networks," *Nano Commun. Netw.*, vol. 1, pp. 3–19, 2010.

[52] Y. Yao, M. A. Kats, P. Genevet, N. Yu, Y. Song, J. Kong, and F. Capasso, "Broad electrical tuning of graphene-loaded plasmonic antennas," *Nano Lett.*, vol. 13, pp. 1257–1264, 2013.

[53] E. Prodan, C. Radloff, N. J. Halas, and P. Nordlander, "A hybridization model for the plasmon response of complex nanostructures," *Science*, vol. 302, pp. 419–422, 2003.

[54] H. Yan, F. Xia, Z. Li, and P. Avouris, "Plasmonics of coupled graphene micro-structures," *New J. Phys.*, vol. 14, p. 125001, 2012.

[55] J. H. Strait, P. S. Nene, W.-M. Chan, C. Manolatou, J. W. Kevek, S. Tiwari, P. L. McEuen, and F. Rana, "Confined plasmons in graphene microstructures: Experiments and theory," *arXiv:1302.5972v2 [cond-mat.mes-hall]*, 2013.

[56] M. V. Fischetti, D. A. Neumayer, and E. A. Cartier, "Effective electron mobility in Si inversion layers in metal–oxide–semiconductor systems with a high-kappa insulator: The role of remote phonon scattering," *J. Appl. Phys.*, vol. 90, pp. 4587–4608, 2001.

[57] M. Freitag, T. Low, W. Zhu, H. Yan, F. Xia, and P. Avouris, "Photocurrent in graphene harnessed by intrinsic, tunable plasmons," *Nat. Commun.*, vol. 4, p. 1951, 2013.

[58] H. Yan, T. Low, W. Zhu, Y. Wu, M. Freitag, X. Li, F. Guinea, P. Avouris, and F. Xia, "Damping pathways of mid-infrared plasmons in graphene nanostructures," *Nat. Photon.*, vol. 7, pp. 394–399, 2013.

[59] M. Jablan, M. Soljacic, and H. Buljan, "Unconventional plasmon-phonon coupling in graphene," *Phys. Rev. B*, vol. 83, p. 161409, 2011.

[60] R. Won, "Graphene metamaterials: Switching terahertz waves," *Nat. Photon.*, vol. 6, pp. 801–801, 2012.

[61] J. H. Davies, *The Physics of Low-Dimensional Semiconductors: An Introduction*. Cambridge, U.K.: Cambridge Univ. Press, 1998.

[62] H. Yan, Z. Li, X. Li, W. Zhu, P. Avouris, and F. Xia, "Infrared spectroscopy of tunable dirac terahertz magneto-plasmons in graphene," *Nano Lett.*, vol. 12, pp. 3766–3771, 2012.

[63] I. Crassee, M. Orlita, M. Potemski, A. L. Walter, M. Ostler, T. Seyller, I. Gaponenko, J. Chen, and A. B. Kuzmenko, "Intrinsic terahertz plasmons and magnetoplasmons in large scale monolayer graphene," *Nano Lett.*, vol. 12, pp. 2470–2474, 2012.

[64] I. Petkovic, F. I. B. Williams, K. Bennaceur, F. Portier, P. Roche, and D. C. Glattli, "Carrier drift velocity and edge magnetoplasmons in graphene," *Phys. Rev. Lett.*, vol. 110, p. 016801, 2013.

[65] E. C. Peters, E. J. Lee, M. Burghard, and K. Kern, "Gate dependent photocurrents at a graphene p-n junction," *Appl. Phys. Lett.*, vol. 97, p. 193102, 2010.

[66] G. Rao, M. Freitag, H.-Y. Chiu, R. S. Sundaram, and P. Avouris, "Raman and photocurrent imaging of electrical stress-induced p-n junctions in graphene," *ACS Nano*, vol. 5, pp. 5848–5854, 2011.

[67] T. Mueller, F. Xia, M. Freitag, J. Tsang, and P. Avouris, "Role of contacts in graphene transistors: A scanning photocurrent study," *Phys. Rev. B*, vol. 79, p. 245430, 2009.

[68] M. Freitag, T. Low, F. Xia, and P. Avouris, "Photoconductivity of biased graphene," *Nat. Photon.*, vol. 7, pp. 53–59, 2013.

[69] D. B. Farmer, R. Golizadeh-Mojarad, V. Perebeinos, Y.-M. Lin, G. S. Tulevski, J. C. Tsang, and P. Avouris, "Chemical doping and electron-hole conduction asymmetry in graphene devices," *Nano Lett.*, vol. 9, pp. 388–392, 2009.

[70] D. Sun, G. Aivazian, A. M. Jones, J. S. Ross, W. Yao, D. Cobden, and X. Xu, "Ultrafast hot-carrier-dominated photocurrent in graphene," *Nat. Nanotechnol.*, vol. 7, pp. 114–118, 2012.

[71] A. Urich, K. Unterrainer, and T. Mueller, "Intrinsic response time of graphene photodetectors," *Nano Lett.*, vol. 11, pp. 2804–2808, 2011.

[72] F. Xia, T. Mueller, Y.-M. Lin, A. Valdes-Garcia, and P. Avouris, "Ultrafast graphene photodetector," *Nat. Nanotechnol.*, vol. 4, pp. 839–843, 2009.

[73] X. Xu, N. M. Gabor, J. S. Alden, A. M. van der Zande, and P. L. McEuen, "Photo-Thermoelectric effect at a graphene interface junction," *Nano Lett.*, vol. 10, pp. 562–566, 2009.

[74] N. M. Gabor, J. C. W. Song, Q. Ma, N. L. Nair, T. Taychatanapat, K. Watanabe, T. Taniguchi, L. S. Levitov, and P. Jarillo-Herrero, "Hot carrier-assisted intrinsic photoresponse in graphene," *Science*, vol. 334, pp. 648–652, 2011.

[75] M. C. Lemme, F. H. L. Koppens, A. L. Falk, M. S. Rudner, H. Park, L. S. Levitov, and C. M. Marcus, "Gate-Activated photoresponse in a graphene p-n junction," *Nano Lett.*, vol. 11, pp. 4134–4137, 2011.

[76] M. Freitag, T. Low, and P. Avouris, "Increased responsivity of suspended graphene photodetectors," *Nano Lett.*, vol. 13, pp. 1644–1648, 2013.

[77] P. A. Obraztsov, G. M. Mikheev, S. V. Garnov, A. N. Obraztsov, and Y. P. Svirko, "Polarization-sensitive photoresponse of nanographite," *Appl. Phys. Lett.*, vol. 98, pp. 091903-1–091903-3, 2011.

[78] S. Bae, H. Kim, Y. Lee, X. Xu, J.-S. Park, Y. Zheng, J. Balakrishnan, T. Lei, H. Ri Kim, Y. I. Song, Y.-J. Kim, K. S. Kim, B. Ozyilmaz, J.-H. Ahn, B. H. Hong, and S. Iijima, "Roll-to-roll production of 30-inch graphene films for transparent electrodes," *Nat. Nanotechnol.*, vol. 5, pp. 574–578, 2010.

[79] S. Bae, S. J. Kim, D. Shin, J. H. Ahn, and B. H. Hong, "Towards industrial applications of graphene electrodes," *Physica. Scripta.*, vol. 2012, p. 014024, 2012.

[80] K. Ellmer, "Past achievements and future challenges in the development of optically transparent electrodes," *Nat. Photon.*, vol. 6, pp. 809–817, 2012.

[81] G. Eda, G. Fanchini, and M. Chhowalla, "Large-area ultrathin films of reduced graphene oxide as a transparent and flexible electronic material," *Nat. Nanotechnol.*, vol. 3, pp. 270–274, 2008.

[82] T.-H. Han, Y. Lee, M.-R. Choi, S.-H. Woo, S.-H. Bae, B. H. Hong, J.-H. Ahn, and T.-W. Lee, "Extremely efficient flexible organic light-emitting diodes with modified graphene anode," *Nat. Photon.*, vol. 6, pp. 105–110, 2012.

[83] J. Wu, H. A. Becerril, Z. Bao, Z. Liu, Y. Chen, and P. Peumans, "Organic solar cells with solution-processed graphene transparent electrodes," *Appl. Phys. Lett.*, vol. 92, pp. 263302-1–263302-3, 2008.

[84] A. Kumar and C. Zhou, "The race to replace tin-doped indium oxide: Which material will win?" *ACS Nano*, vol. 4, pp. 11–14, 2010.

[85] T. Kobayashi, M. Bando, N. Kimura, K. Shimizu, K. Kadono, N. Umezu, K. Miyahara, S. Hayazaki, S. Nagai, Y. Mizuguchi, Y. Murakami, and D. Hobara, "Production of a 100-m-long high-quality graphene transparent conductive film by roll-to-roll chemical vapor deposition and transfer process," *Appl. Phys. Lett.*, vol. 102, pp. 023112-1–023112-4, 2013.

[86] V. B. Bregar, "Advantages of ferromagnetic nanoparticle composites in microwave absorbers," *IEEE Trans. Magn.*, vol. 40, no. 3, pp. 1679–1684, May 2004.

[87] Z. Han, D. Li, H. Wang, X. G. Liu, J. Li, D. Y. Geng, and Z. D. Zhang, "Broadband electromagnetic-wave absorption by FeCo/C nanocapsules," *Appl. Phys. Lett.*, vol. 95, pp. 023114-1–023114-3, 2009.

[88] Q. Bao, H. Zhang, B. Wang, Z. Ni, C. H. Y. X. Lim, Y. Wang, D. Y. Tang, and K. P. Loh, "Broadband graphene polarizer," *Nat. Photon.*, vol. 5, pp. 411–415, 2011.

[89] Q. Bao, H. Zhang, Y. Wang, Z. Ni, Y. Yan, Z. X. Shen, K. P. Loh, and D. Y. Tang, "Atomic-Layer graphene as a saturable absorber for ultrafast pulsed lasers," *Adv. Functional Mater.*, vol. 19, pp. 3077–3083, 2009.

[90] Z. Sun, T. Hasan, F. Torrisi, D. Popa, G. Privitera, F. Wang, F. Bonaccorso, D. M. Basko, and A. C. Ferrari, "Graphene mode-locked ultrafast laser," *ACS Nano*, vol. 4, pp. 803–810, 2010.

[91] W. D. Tan, C. Y. Su, R. J. Knize, G. Q. Xie, L. J. Li, and D. Y. Tang, "Mode locking of ceramic Nd:yttrium aluminum garnet with graphene as a saturable absorber," *Appl. Phys. Lett.*, vol. 96, pp. 031106-1–031106-3, 2010.

[92] H. Zhang, D. Y. Tang, L. M. Zhao, Q. L. Bao, and K. P. Loh, "Large energy mode locking of an erbium-doped fiber laser with atomic layer graphene," *Opt. Exp.*, vol. 17, pp. 17630–17635, 2009.

[93] M. Liu, X. Yin, E. Ulin-Avila, B. Geng, T. Zentgraf, L. Ju, F. Wang, and X. Zhang, "A graphene-based broadband optical modulator," *Nature*, vol. 474, pp. 64–67, 2011.

[94] M. Liu, X. Yin, and X. Zhang, "Double-Layer graphene optical modulator," *Nano Lett.*, vol. 12, pp. 1482–1485, 2012.

[95] X. Gan, R.-J. Shiue, Y. Gao, K. F. Mak, X. Yao, L. Li, A. Szep, D. Walker, J. Hone, T. F. Heinz, and D. Englund, "High-Contrast electrooptic modulation of a photonic crystal nanocavity by electrical gating of graphene," *Nano Lett.*, vol. 13, pp. 691–696, 2013.

[96] B. Sensale-Rodriguez, T. Fang, R. Yan, M. M. Kelly, D. Jena, L. Liu, and H. Xing, "Unique prospects for graphene-based terahertz modulators," *Appl. Phys. Lett.*, vol. 99, pp. 113104-1–113104-3, 2011.

[97] T. Mueller, F. Xia, and P. Avouris, "Graphene photodetectors for high-speed optical communications," *Nat. Photon.*, vol. 4, pp. 297–301, 2010.

[98] M. Engel, M. Steiner, A. Lombardo, A. C. Ferrari, H. v. Loehneysen, P. Avouris, and R. Krupke, "Light-matter interaction in a microcavity-controlled graphene transistor," *Nat. Commun.*, vol. 3, p. 906, 2012.

[99] M. Furchi, A. Urich, A. Pospischil, G. Lilley, K. Unterrainer, H. Detz, P. Klang, A. M. Andrews, W. Schrenk, G. Strasser, and T. Mueller, "Microcavity-integrated graphene photodetector," *Nano Lett.*, vol. 12, pp. 2773–2777, 2012.

[100] A. Pospischil, M. Humer, M. M. Furchi, R. Guider, T. Fromherz, and T. Mueller, "CMOS-integrated graphene photodetector covering all optical communication bands," *arXiv:1302.3854 [cond-mat.mes-hall]*, 2013.

[101] J. Liu, J. Michel, W. Giziewicz, D. Pan, K. Wada, D. D. Cannon, S. Jongthammanurak, D. T. Danielson, L. C. Kimerling, J. Chen, F. O. Ilday, F. X. Kartner, and J. Yasaitis, "High-performance, tensile-strained Ge p-i-n photodetectors on a Si platform," *Appl. Phys. Lett.*, vol. 87, pp. 103501-1–103501-3, 2005.

[102] M. W. Geis, S. J. Spector, M. E. Grein, R. T. Schulein, J. U. Yoon, D. M. Lennon, S. Deneault, F. Gan, F. X. Kaertner, and T. M. Lyszczarz, "CMOS-compatible All-Si high-speed waveguide photodiodes with high responsivity in near-infrared communication band," *IEEE Phot. Technol. Lett.*, vol. 19, pp. 152–154, 2007.

[103] T. J. Echtermeyer, L. Britnell, P. K. Jasnos, A. Lombardo, R. V. Gorbachev, A. N. Grigorenko, A. K. Geim, A. C. Ferrari, and K. S. Novoselov, "Strong plasmonic enhancement of photovoltage in graphene," *Nat. Commun.*, vol. 2, p. 458, 2011.

[104] Z. Fang, Z. Liu, Y. Wang, P. M. Ajayan, P. Nordlander, and N. J. Halas, "Graphene-Antenna sandwich photodetector," *Nano Lett.*, vol. 12, pp. 3808–3813, 2012.

[105] G. Konstantatos, M. Badioli, L. Gaudreau, J. Osmond, M. Bernechea, F. P. G. de Arquer, F. Gatti, and F. H. L. Koppens, "Hybrid graphene-quantum dot phototransistors with ultrahigh gain," *Nat. Nanotechnol.*, vol. 7, pp. 363–368, 2012.

[106] J. Yan, M. H. Kim, J. A. Elle, A. B. Sushkov, G. S. Jenkins, H. M. Milchberg, M. S. Fuhrer, and H. D. Drew, "Dual-gated bilayer graphene hot-electron bolometer," *Nat. Nanotechnol.*, vol. 7, pp. 472–478, 2012.

[107] F. Xia, D. B. Farmer, Y.-m. Lin, and P. Avouris, "Graphene field-effect transistors with high on/off current ratio and large transport band gap at room temperature," *Nano Lett.*, vol. 10, pp. 715–718, 2010.

[108] Y. Zhang, T.-T. Tang, C. Girit, Z. Hao, M. C. Martin, A. Zettl, M. F. Crommie, Y. R. Shen, and F. Wang, "Direct observation of a widely tunable bandgap in bilayer graphene," *Nature*, vol. 459, pp. 820–823, 2009.

[109] H. Vora, P. Kumaravadivel, B. Nielsen, and X. Du, "Bolometric response in graphene based superconducting tunnel junctions," *Appl. Phys. Lett.*, vol. 100, p. 153507, 2012.
[110] K. C. Fong and K. C. Schwab, "Ultrasensitive and wide-bandwidth thermal measurements of graphene at low temperatures," *Phys. Rev. X*, vol. 2, p. 031006, 2012.
[111] L. Vicarelli, M. S. Vitiello, D. Coquillat, A. Lombardo, A. C. Ferrari, W. Knap, M. Polini, V. Pellegrini, and A. Tredicucci, "Graphene field-effect transistors as room-temperature terahertz detectors," *Nat. Mater.*, vol. 11, pp. 865–871, 2012.
[112] F. Rana, "Graphene terahertz plasmon oscillators," *IEEE Trans. Nanotechnol.*, vol. 7, pp. 91–99, 2008.
[113] G. Ramakrishnan, R. Chakkittakandy, and P. C. M. Planken, "Terahertz generation from graphite," *Opt. Exp.*, vol. 17, pp. 16092–16099, 2009.
[114] L. Prechtel, L. Song, D. Schuh, P. Ajayan, W. Wegscheider, and A. W. Holleitner, "Time-resolved ultrafast photocurrents and terahertz generation in freely suspended graphene," *Nat. Commun.*, vol. 3, p. 646, 2012.

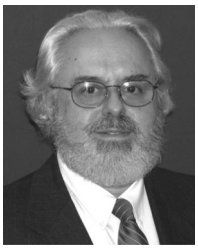

Phaedon Avouris received the B.Sc. degree from the Aristotle University, Thessaloniki, Greece and the Ph.D. degree in physical chemistry from Michigan State University in 1974. He did postdoctoral work at the University of California, Los Angeles, CA, USA and was a Research Fellow at AT&T Bell Laboratories before joining the staff of IBM's Research Division at the Watson Research Center in 1978. He is currently an IBM Fellow and the Manager of Nanoscience and Nanotechnology at the T. J. Watson Research Center, Yorktown Heights, NY, USA. Dr. Avouris has published about 500 scientific papers. He has been elected Fellow of the American Academy of Arts and Sciences, the American Physical Society, the Institute of Physics of the U.K., the National Academy of Greece, the IBM Academy of Technology, Materials Research Society, American Association for the Advancement of Science, the New York Academy of Sciences, and the American Vacuum Society. He has received many awards including the APS Irving Langmuir Prize for Chemical Physics, the IEEE Nanotechnology Pioneer Award, the MRS David Turnbull Lectureship, the AVS Medard W. Welch Award for Surface Science, the Julius Springer Award for Applied Physics, the Richard E. Smalley Research Award of the Electrochemical Society, and the Richard Feynman Nanotechnology Prize. He has also received many IBM Corporate and Outstanding Technical Achievement awards.

Marcus Freitag received the Diplom degree from the University of Tuebingen, Tuebingen Germany, in 1998, the M.S. degree from the University of Massachusetts Boston, Boston, MA, USA, in 1995, and the Ph.D. degree in physics from the University of Pennsylvania, Philadelphia, PA, USA, in 2002. After postdoctoral work for Carbon Nanotechnologies, Inc., he joined the Research Division of IBM in 2004. He is currently a Research Staff Member in the Nanoscience and Nanotechnology group, IBM T.J. Watson Research Center, Yorktown Heights, NY, USA. He has previously worked on scanning probe microscopy and electronic transport in carbon nanotubes. He is currently focusing on optoelectronics in graphene. Dr. Freitag has published more than 50 scientific papers. He has authored and coauthored several book chapters and reviews on carbon nanotube and graphene electronics and optoelectronics. He is a Member of the American Physical Society.